Chemical Science

Dynamic Article Links ►

Cite this: DOI: 10.1039/c0xx00000x

www.rsc.org/xxxxxx

ARTICLE TYPE

Capping Nanoparticles with Graphene Quantum Dots for Enhanced Thermoelectric Performance

Yuantong Liang[1,2], Chenguang Lu[1*], Defang Ding[1], Man Zhao[1], Dawei Wang[1], Chao Hu[3], Jieshan Qiu[3], Gang Xie[2*], Zhiyong Tang[1*]

Received (in XXX, XXX) Xth XXXXXXXXX 20XX, Accepted Xth XXXXXXXXX 20XX
DOI: 10.1039/b000000x

ABSTRACT Graphene quantum dot (GQD) was shown to serve as a phase transfer agent to transfer varying types of nanoparticles (NPs) from non-polar solvent into polar solvent. Thorough characterization of the NPs proves a complete removal of native ligands. Pellets from this GQD-NP composite show GQD limits crystalline size of NP during spark plasma sintering, and yield enhanced thermoelectric performance when compared with NPs exchanged with conventional inorganic ions. Photoluminescence study on this composite also suggests energy transfer from GQDs to NPs.

Introduction

Inorganic nanoparticles (NPs) deliver many unique properties that have attracted much attention since they were introduced[1]. However, the most versatile wet-chemistry synthetic methods for the NPs inevitably coat them with long chain organic ligands, which insulate the NPs from each other and their environment. Removal of such organic coatings thus becomes a key challenge for incorporating NPs into devices as functional parts. Many agents have been proposed to replace the native ligands, including inorganic anions[2-4], chalcogenide complex[5, 6], $NOBF_4$[7], Meerwein salt[8], formic acid[9, 10], thiolate ligands[11-14], and polymers[15, 16]. These agents effectively strip the native ligands of NPs and bring them closer, causing the improved electric conductivity or energy transfer. However, these replacing ligands, except for metal chalcogenide complex and polymers, are mostly small chemical species and serve as stabilizing agents only.

Recent advance on nanocomposite materials presents a scalable methodology of generating multifunctional materials with properties stemming from individual components and, more interestingly, their synergistic interactions[17-22]. When incorporating NPs in such nanocomposites, for the sake of property versatility, one would desire a ligand beyond just colloidal stabilization, i.e., a ligand with functionalities. Herein, we present to use graphene quantum dots (GQDs) as the ligands to stabilize nanoparticles.

GQDs can be viewed as a derivative of the extensively studied two-dimensional material, graphene[23-27]. They are a class of nanometer-sized graphitic sheets with abundant edge functional groups[28, 29]. The size-related band gap and photoluminescence (PL) property have permitted their application in bio-labeling[29, 30].

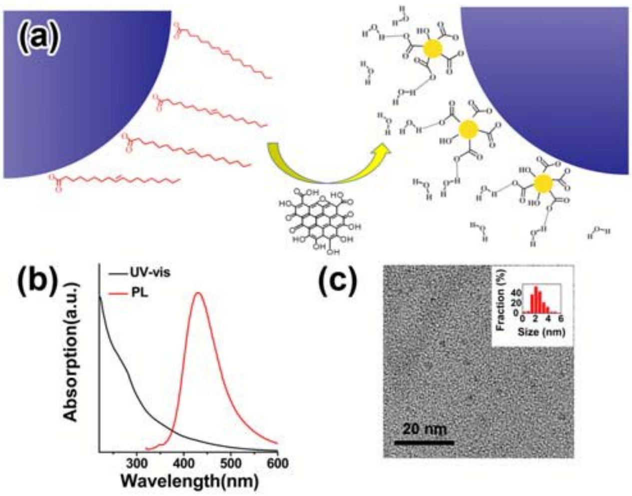

Figure 1. a) Schematic drawing of using GQDs as capping ligands to replace native oleic acid. b) UV-Vis and photoluminescence spectra of GQDs. c) TEM image of GQDs. Inset presents the histogram of the size distribution of GQDs.

Recent incorporation of GQDs into nanocomposite materials also offers the opportunity to take advantage of their unique charge carrier extraction capability for better solar cell efficiency[31, 32]. In this communication, we demonstrate that GQDs can be used directly as a native-ligand exchanger and stabilize NPs in polar solvents (Figure 1a)[33]. We further show that, when the composite is made into pellet by spark plasma sintering (SPS), the fusing-up of NPs is lessoned and a significantly enhanced thermoelectric performance is acquired, likely due to preserved quantum confinement and carrier energy filtering[34, 35]. This novel type of GQD ligands is thus advantageous over conventional molecular ligands when high temperature stability of ligands is needed.

Results and Discussion

Inorganic NPs were made through well-developed wet-chemistry methods[36-39]. For GQDs synthesis, graphene oxide (GO) from natural graphite powder was first prepared by a modified Hummer's method[40], and hydrothermal method was then adopted to cut GO into small pieces of GQDs[41, 42] (Details in SI). As-synthesized GQDs are highly luminescent with a PL peak at 440 nm (Figure 1b), while transmission electron microscopy (TEM) imaging shows the GQDs with uniform sizes of around 2.5 nm (Figure 1c), proving them to be of high quality. The ligand exchange processes were carried out in a nitrogen-filled glovebox. For a typical ligand exchange, 3 mL of NPs in toluene solution was added to 3 mL of GQDs in formamide and vigorous stirred for several hours. After complete phase transfer, the toluene phase was discarded, and the formamide phase was washed three times with fresh toluene. The resulting GQD-NPs were precipitated by acetone and finally redispersed in DMF or DMSO.

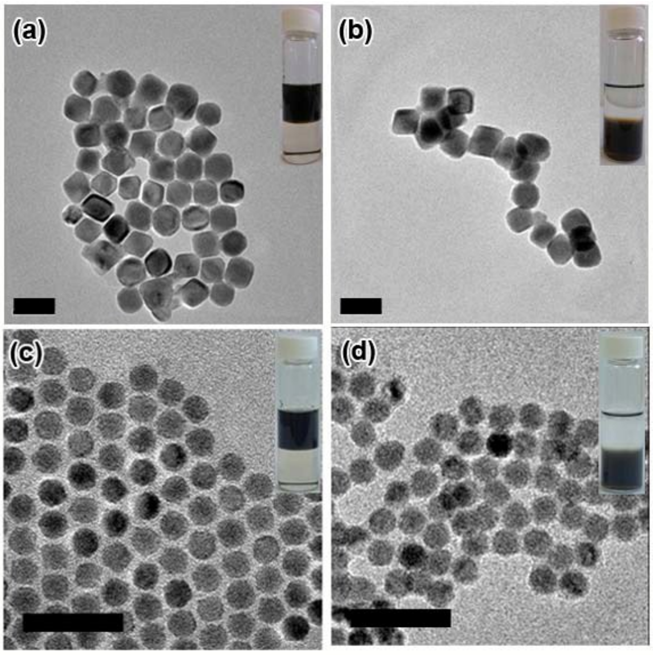

Figure 2. TEM images of Pb-based NPs before (a, c) and after (b, d) GQD ligand exchange. (a, b) PbTe, 30 nm; (c, d) PbSe, 10 nm. The scale bars are 50 nm. Insets are photos of NPs dispersed in top non-polar phase toluene and bottom polar phase formamide with GQDs.

The insets in Figure 2 and S1 present photographs of transferring the NPs from non-polar phase (top phase) into polar phase (bottom phase) with aid of GQDs. The transfer starts upon contact of the GQDs-containing polar phase with NPs in toluene. Pb-based NPs are readily transferred within hours, while Cd-based NPs needs slightly longer time to accomplish the transfer, demonstrating the universality of GODs as phase transfer agent. Also, the difference could be attributed to different affinity of surface cations (Pb vs. Cd) with GQDs. The TEM images before and after phase transfer indicate that the NPs preserve their shape and size (Figure 2). Thermal gravity analysis displays that as for 18 nm PbTe NPs, weight loss is 17% before GQD exchange and 8% after GQD exchange (Figure S2). By comparing the final residue weight of GQD-PbTe nanocomposites and that of pure GQDs, we could estimate that the weight percentage of GQDs in this composite is about 14%.

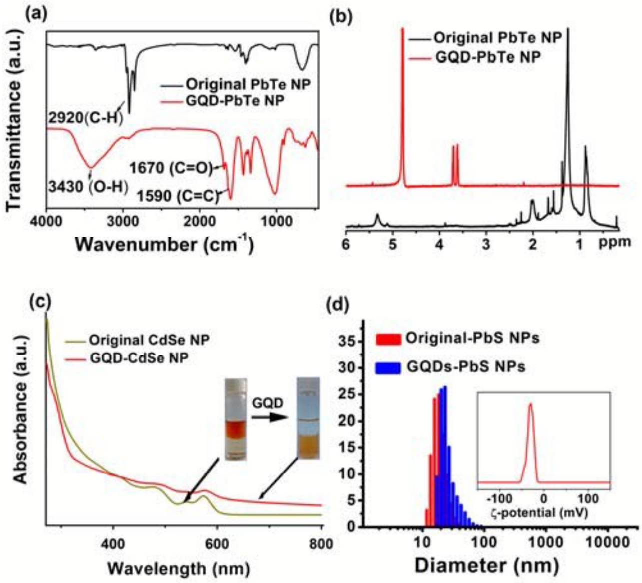

Figure 3. a) FTIR spectra and b) 1H NMR spectra of PbTe NPs before and after ligand exchange; c) UV-Vis spectra of CdSe NPs before and after ligand exchange. The first exciton peak of NPs is preserved, while GQD absorption feature near 287 nm is observed. It indicates that NP core structures are preserved during the ligand exchange. d) Size distribution of PbS NPs before (red) and after (blue) GQD ligand exchange. Insets are their ζ-potentials after GQD ligand exchange.

The Fourier transform infrared spectroscopy (FTIR) spectrum of the NP dispersion after phase transfer shows greatly reduced peak for C-H stretch mode at ~2900 cm^{-1} (Figure 3a and Figure S3), confirming the removal of alkyl chains on the surface of NPs. The peaks at 1670 cm^{-1} and 1590 cm^{-1} are assigned to stretch modes for C=O and C=C, respectively, indicating GQD's presence after ligand exchange. Furthermore, ^{1}H nuclear magnetic resonance (NMR) spectroscopy clearly proves exclusive removal of alkyl H atoms in the range of 0.8 - 2.5 ppm and alkene H atoms at 5.3 ppm (Figure 3b and Figure S4), and the chemical shifts at 3.6 ppm and 3.7 ppm of GQD-NPs are assigned to the two types of H atoms on GQDs (Figure S4). These spectroscopic evidences are consistent with the proposed scheme (Figure 1a) in which the native ligands of NPs are totally stripped by GQDs after phase transfer.

X-ray diffraction (XRD) patterns for PbTe NPs before and after GQD ligand exchange are shown in Figure S5a. Evidently, there is no observable change in the structure integrity for NPs during the phase transfer process. UV-Vis spectroscopy of CdSe NPs before and after GQD ligand exchange further reveals no obvious shifting in the first exciton peak (Figure 3c), and HRTEM image (figure S6) also suggests no modification of the NP cores upon GQDs coating.

It would be interesting to learn how GQDs are assembled near the surface of NPs to form a stable dispersion in polar solvent. We therefore performed dynamic light scattering (DLS) study to reveal this behaviour *in situ*. Figure 3d displays that the GQD-PbS NP complexes are dispersed in DMSO with a uniform hydrodynamic diameter slightly larger than that of the original NPs with organic ligands. This could be explained by the larger size of the solvation shells containing GQDs and polar solvent molecules, when compared to the native oleic acid. It should be noted that such shells collapse due to loss of solvent in TEM chamber, which result in a closer inter-NP distance in Figure 2. All these complexes formed stable colloidal solution and were stored in ambient condition for more than 3 month without noticeable changes. The negatively charged surfaces (negative ζ-potential in the insets of Figure 3d and S5b) suggest that the GQDs are grafted onto NP surfaces with some of their carboxylic groups, and the other carboxylic groups facing to the polar solvent are deprotonated to stabilize the NPs with solvation energy. The proposed scenario is presented in Figure 1a. It should be noted that the small sizes of GQDs limit us from obtaining more *in situ* details of GQD status in the GQD-NP complexes, which still remains a major challenge for almost all types of ligands on the NP surfaces.

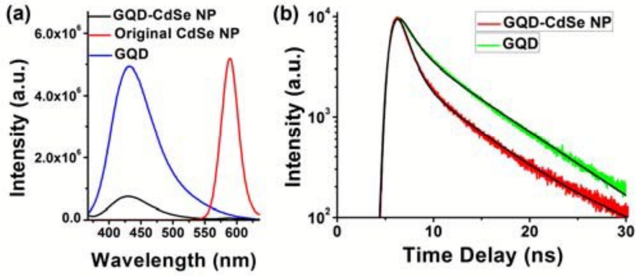

Figure 4. a) PL of GQDs alone (blue), CdSe NPs alone (red), and GQDs capping CdSe NPs (black), showing dramatically quenched emission of both CdSe NPs and GQDs in the composite. b) Transient spectroscopy of GQDs PL emission. For the two major decay branches, lifetimes of GQDs alone are τ_1 = 1.34 ns and τ_2 = 6.77 ns, while lifetimes of GQDs liganding CdSe NPs are τ_1 = 0.98 ns and τ_1 = 6.56 ns.

To further prove the binding of GQD onto NPs, we studied PL of the GQD capped CdSe NP dispersed in solution (Figure 4) [43, 44]. CdSe NPs are selected because their emission is located in the visible range and easily measured. The PL intensity of GQDs after binding with the NPs is decreased by ~90%, and the life times, for the two major decay branches, are reduced from τ_1 = 1.34 ns and τ_2 = 6.77 ns to τ_1 = 0.98 ns and τ_2 = 6.56 ns, respectively (Figure 4b), which suggest occurrence of short distance energy transfer from GQDs to CdSe NP cores. Meanwhile, emission of CdSe NPs is almost completely quenched. We compared high resolution TEM (Figure S6) for CdSe NPs before and after GQD ligand exchange and found no obvious change in their crystallinity, which indicates that the PL quenching of CdSe NPs is caused by poor surface trap passivation instead of core structural change. We suppose that passivation of CdSe NP surface traps with wide-band-gap shells such as ZnS would preserve PL characteristics of CdSe NPs and allows us to better elucidate the energy transfer between GQDs and CdSe NPs. Such detailed study is underway for deeper understanding of the energy flow in this composite material. The spectroscopy result indicates that GQDs are bound to the surface of NPs and serves as a ligand, instead of free floating in the solution. Such interaction and energy transfer between GQD ligands and NP cores would also permit engineering of versatile property from this type of composite towards functional materials.

Composites made from NPs are promising materials for thermoelectric application, because of their inherent low thermal conductivity and enhanced Seebeck coefficients from quantum confining and energy filtering effects.[35] However, NPs generally suffer from alloying and fusing up at elevated temperature, causing weakening of such effects and irreversibly decreased Seebeck coefficient.[45, 46] By capping the PbTe NPs with GQDs, we demonstrate that the thermally stable GQDs could effectively lesson sintering of NPs in the composite. We made pellets (Figure S7) from GQD (from coal oxidation, see SI) capped PbTe NPs by SPS for thermoelectric measurement. As comparison, the control pellets were also prepared with PbTe NPs capped by the most common ligands, SCN anions, which would decompose into gaseous species at the SPS temperature of 450°C[3, 47]. Scanning electron microscopy (SEM) images of the cross sections of these two pellets reveal that much finer nanostructures exist in the pellet from GQDs capped NPs than those from SCNs capped NPs (Figure 5a and 5b). XRD diffraction pattern also confirms that the PbTe crystalline domain size is smaller in the former composite (Figure S8 and Table S1). GQD's presence after SPS was confirmed by Raman spectrum (shown in Figure S7b), indicating its thermal stability. The above observations suggest that the capping GQDs around PbTe NPs lesson their fusing-up and keep the crystalline domains smaller. Such effect would benefit thermoelectric properties with enhanced Seebeck coefficients from nanostructuring.

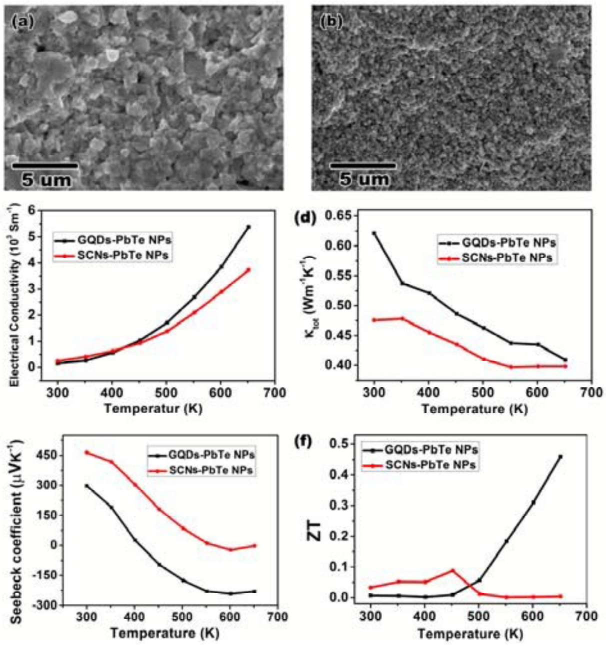

Figure 5. The cross-section SEM images of pellets of SCNs-PbTe NPs, (a), and GQDs-PbTe NPs, (b), by SPS. The measured electrical conductivity, (c), thermal conductivity, (d), Seebeck coefficient, (e), and calculated ZT values, (f), are presented as a function of temperature.

The thermoelectric measurement highlights advantages of using GQDs over SCNs as capping agents for both electric conductivity and Seebeck coefficient (Figure 5c-5f). The final calculated figure of merit (ZT) shows a peak value of 0.46 at 650K for GQD-PbTe NP complex, which is among the best for solution processed pure PbTe thermoelectric materials[48-50]. Numerically, the main reason for the good ZT is attributed to an enhanced n-type Seebeck coefficient at 650K. The switching of conduction type from p to n for both pellets can be understood as excitation of electrons in the composite at elevated temperature.

Interestingly, the GQDs capped NP complex shows a much quicker conduction-type switch and a higher Seebeck coefficient value when a plateau is reached (Figure 5e). The mechanisms to account for such enhanced Seebeck coefficient could be complicated. Besides the aforementioned quantum confining effect, electron doping and carrier filtering effect of GQDs could also play roles, since a heterojunction formed between GQDs and the PbTe matrix. More detailed studies, therefore, are needed to understand the thermoelectric behaviour of the GQD-PbTe composite. Nevertheless, the GQDs capped NP complex shows a considerable ZT value even without tuning of composition and doping of the NPs,[51] which suggests a good candidate for thermoelectrics. Given the thermal stability of GQDs, it is also advantageous over molecular capping ligands for controlling crystalline size for optimized thermoelectric properties.

The prepared GQD-NP composite could see other applications when collective properties of different components are desired. We have demonstrated the effect of GQDs in lessoning sintering of PbTe NPs for enhanced thermoelectric performance. Another application is likely to be photovoltaic materials. There are reports of mixing GQDs with TiO_2 NPs[44, 52] or ZnO nanowires[53] to improve solar cell performance by taking advantages of energy transfer between GQDs and other nanomaterials. The tunable band structure of GQDs together with their good interfacing with NPs allows one to fine tune such energy transfer between GQDs and NPs in hope of yielding novel properties of the composite, which is also superior to molecular ligands. Recent progress on making mass scale GQDs[26, 54, 55] will permit mass production of these GQD-NP composites for industrial applications.

Conclusions

In conclusion, for the first time, we reported the general capability of GQDs to serve as a capping ligand to exchange the native organic stabilizer on varying types of semiconductor NPs. FTIR, NMR, TEM and XRD characterization results have proved that the ligand exchange is complete and the integrity of NPs is preserved. Thermoelectric measurement of GQD-PbTe composite reveals that the GQDs play a crucial role of limiting crystalline size for enhanced Seebeck coefficient, and thus a considerable ZT value of 0.46 is obtained even without tuning composition/doping level of NPs. Study on PL lifetime of the GQD-NPs shows efficient energy transfer between the GQD ligands and the NP cores. Given the abundant yet tunable properties of GQDs, one would anticipate that versatile properties could originate from the novel type of GQD-NP composites and benefit various applications, such as photovoltaics, catalysts, and thermoelectrics.

Notes and references

1 CAS Key Lab for Nanosystem and Hierarchy Fabrication, National Center for Nanoscience and Technology, Beijing, 100190 China
2 Key Laboratory of Synthesis and Natural Functional Molecular Chemistry of Ministry of Education, College of Chemistry & Materials Science, Northwest University, Xi'an, 710069 China
3 Carbon Research Laboratory, Center for Nano Materials and Science, State Key Laboratory of Fine Chemicals, School of Chemical Engineering and Key Laboratory for Micro/Nano Technology of Liaoning Province, Dalian University of Technology, Dalian 116024 China

** Prof. C. Lu, Email: lucg@nanoctr.cn; Prof. G. Xie, Email: xiegang@nwu.edu.cn ; Prof. Z. Tang, Email: zytang@nanoctr.cn*

† Electronic Supplementary Information (ESI) available: [details of any supplementary information available should be included here]. See DOI: 10.1039/b000000x/

ACKNOWLEDGMENT
The authors thank funding support from NSFC (No. 21025310 and 51372028), the Instrument Developing Project of the Chinese Academy of Sciences (No.YZ201311), the CAS-CSIRO Cooperative Research Program (No. GJHZ1503). The authors thank Prof. Y. Li for helpful discussion, H. Yin, C. Yang, Y. Zheng, Y. Chen, Dr. Li, and Prof. S. Zheng for experimental assistance.

Notes and References

1. Heiligtag, F. J.; Niederberger, M. The Fascinating World of Nanoparticle Research. *Mater. Today* **2013**, *16*, 262-271.
2. Nag, A.; Kovalenko, M. V.; Lee, J.-S.; Liu, W.; Spokoyny, B.; Talapin, D. V. Metal-Free Inorganic Ligands for Colloidal Nanocrystals: S^{2-}, HS^-, Se^{2-}, HSe^-, Te^{2-}, HTe^-, TeS_3^{2-}, OH^-, and NH^{2-} as Surface Ligands. *J. Am. Chem. Soc.* **2011**, *133*, 10612-10620.
3. Fafarman, A. T.; Koh, W.-k.; Diroll, B. T.; Kim, D. K.; Ko, D.-K.; Oh, S. J.; Ye, X.; Doan-Nguyen, V.; Crump, M. R.; Reifsnyder, D. C.; Murray, C. B.; Kagan, C. R. Thiocyanate-Capped Nanocrystal Colloids: Vibrational Reporter of Surface Chemistry and Solution-Based Route to Enhanced Coupling in Nanocrystal Solids. *J. Am. Chem. Soc.* **2011**, *133*, 15753-15761.
4. Zhang, H.; Hu, B.; Sun, L.; Hovden, R.; Wise, F. W.; Muller, D. A.; Robinson, R. D. Surfactant Ligand Removal and Rational Fabrication of Inorganically Connected Quantum Dots. *Nano Lett.* **2011**, *11*, 5356-5361.
5. Buckley, J. J.; Couderc, E.; Greaney, M. J.; Munteanu, J.; Riche, C. T.; Bradforth, S. E.; Brutchey, R. L. Chalcogenol Ligand Toolbox for CdSe Nanocrystals and Their Influence on Exciton Relaxation Pathways. *ACS Nano* **2014**, *8*, 2512-2521.
6. Kovalenko, M. V.; Scheele, M.; Talapin, D. V. Colloidal Nanocrystals with Molecular Metal Chalcogenide Surface Ligands. *Science* **2009**, *324*, 1417-1420.
7. Dong, A.; Ye, X.; Chen, J.; Kang, Y.; Gordon, T.; Kikkawa, J. M.; Murray, C. B. A Generalized Ligand-Exchange Strategy Enabling Sequential Surface Functionalization of Colloidal Nanocrystals. *J. Am. Chem. Soc.* **2011**, *133*, 998-1006.
8. Rosen, E. L.; Buonsanti, R.; Llordes, A.; Sawvel, A. M.; Milliron, D. J.; Helms, B. A. Exceptionally Mild Reactive Stripping of Native Ligands from Nanocrystal Surfaces by Using Meerwein's Salt. *Angewandte Chemie-International Edition* **2012**, *51*, 684-689.
9. Dong, A.; Jiao, Y.; Milliron, D. J. Electronically Coupled Nanocrystal Super lattice Films by in Situ Ligand Exchange at the Liquid-Air Interface. *Acs Nano* **2013**, *7*, 10978-10984.
10. Zarghami, M. H.; Liu, Y.; Gibbs, M.; Gebremichael, E.; Webster, C.; Law, M. p-Type PbSe and PbS Quantum Dot Solids Prepared with Short-Chain Acids and Diacids. *ACS Nano* **2010**, *4*, 2475-2485.
11. Deng, Z.; Cao, D.; He, J.; Lin, S.; Lindsay, S. M.; Liu, Y. Solution Synthesis of Ultrathin Single-Crystalline SnS Nanoribbons for Photodetectors via Phase Transition and Surface Processing. *ACS Nano* **2012**, *6*, 6197-6207.
12. Qin, B.; Zhao, Z.; Song, R.; Shanbhag, S.; Tang, Z. A Temperature-Driven Reversible Phase Transfer of 2-(Diethylamino)ethanethiol-Stabilized CdTe Nanoparticles. *Angew. Chem. Int. Ed.* **2008**, *47*, 9875-9878.
13. Owen, J. S.; Park, J.; Trudeau, P.-E.; Alivisatos, A. P. Reaction Chemistry and Ligand Exchange at Cadmium−Selenide Nanocrystal Surfaces. *J. Am. Chem. Soc.* **2008**, *130*, 12279-12281.
14. Luther, J. M.; Law, M.; Song, Q.; Perkins, C. L.; Beard, M. C.; Nozik, A. J. Structural, Optical, and Electrical Properties of Self-Assembled Films of PbSe Nanocrystals Treated with 1,2-Ethanedithiol. *ACS Nano* **2008**, *2*, 271-280.

15. Zhao, L.; Lin, Z. Crafting Semiconductor Organic−Inorganic Nanocomposites via Placing Conjugated Polymers in Intimate Contact with Nanocrystals for Hybrid Solar Cells. *Adv. Mater.* **2012**, *24*, 4353-4368.
16. Ehrler, B.; Wilson, M. W. B.; Rao, A.; Friend, R. H.; Greenham, N. C. Singlet Exciton Fission-Sensitized Infrared Quantum Dot Solar Cells. *Nano Lett.* **2012**, *12*, 1053-1057.
17. Cao, X.; Yin, Z.; Zhang, H. Three-Dimensional Graphene Materials: Preparation, Structures and Application in Supercapacitors. *Energ. Environ. Sci.* **2014**, *7*, 1850-1865.
18. Milliron, D. J.; Buonsanti, R.; Llordes, A.; Helms, B. A. Constructing Functional Mesostructured Materials from Colloidal Nanocrystal Building Blocks. *Acc. Chem. Res.* **2013**, *47*, 236-246.
19. Llordes, A.; Garcia, G.; Gazquez, J.; Milliron, D. J. Tunable Near-Infrared and Visible-Light Transmittance in Nanocrystal-in-Glass Composites. *Nature* **2013**, *500*, 323-326.
20. Cheng, Y.; Lu, S.; Zhang, H.; Varanasi, C. V.; Liu, J. Synergistic Effects from Graphene and Carbon Nanotubes Enable Flexible and Robust Electrodes for High-Performance Supercapacitors. *Nano Lett.* **2012**, *12*, 4206-4211.
21. Mao, Z.; Guo, J.; Bai, S.; Nguyen, T.-L.; Xia, H.; Huang, Y.; Mulvaney, P.; Wang, D. Hydrogen-Bond-Selective Phase Transfer of Nanoparticles across Liquid/Gel Interfaces. *Angew. Chem. Int. Ed.* **2009**, *48*, 4953-4956.
22. Lu, C.; Akey, A.; Wang, W.; Herman, I. P. Versatile Formation of CdSe Nanoparticle-Single Walled Carbon Nanotube Hybrid Structures. *J. Am. Chem. Soc.* **2009**, *131*, 3446-3447.
23. Tan, C.; Huang, X.; Zhang, H. Synthesis and Applications of Graphene-Based Noble Metal Nanostructures. *Mater. Today* **2013**, *16*, 29-36.
24. Huang, X.; Qi, X.; Boey, F.; Zhang, H. Graphene-Based Composites. *Chem. Soc. Rev.* **2012**, *41*, 666-686.
25. Huang, X.; Yin, Z.; Wu, S.; Qi, X.; He, Q.; Zhang, Q.; Yan, Q.; Boey, F.; Zhang, H. Graphene-Based Materials: Synthesis, Characterization, Properties, and Applications. *Small* **2011**, *7*, 1876-1902.
26. Hu, C.; Yu, C.; Li, M.; Wang, X.; Yang, J.; Zhao, Z.; Eychmüller, A.; Sun, Y. P.; Qiu, J. Chemically Tailoring Coal to Fluorescent Carbon Dots with Tuned Size and Their Capacity for Cu(II) Detection. *Small* **2014**, *10*, 4926-4933.
27. Schultz, B. J.; Patridge, C. J.; Lee, V.; Jaye, C.; Lysaght, P. S.; Smith, C.; Barnett, J.; Fischer, D. A.; Prendergast, D.; Banerjee, S. Imaging local electronic corrugations and doped regions in graphene. *Nat. Commun.* **2011**, *2*, 372.
28. Yan, X.; Li, B.; Li, L.-s. Colloidal Graphene Quantum Dots with Well-Defined Structures. *Acc. Chem. Res.* **2012**, *46*, 2254-2262.
29. Shen, J.; Zhu, Y.; Yang, X.; Li, C. Graphene Quantum Dots: Emergent Nanolights for Bioimaging, Sensors, Catalysis and Photovoltaic Devices. *Chem. Commun.* **2012**, *48*, 3686-3699.
30. Qian, J.; Wang, D.; Cai, F.-H.; Xi, W.; Peng, L.; Zhu, Z.-F.; He, H.; Hu, M.-L.; He, S. Observation of Multiphoton-Induced Fluorescence from Graphene Oxide Nanoparticles and Applications in In Vivo Functional Bioimaging. *Angew. Chem. Int. Ed.* **2012**, *51*, 10570-10575.
31. Zhu, Z.; Ma, J.; Wang, Z.; Mu, C.; Fan, Z.; Du, L.; Bai, Y.; Fan, L.; Yan, H.; Phillips, D. L.; Yang, S. Efficiency Enhancement of Perovskite Solar Cells through Fast Electron Extraction: The Role of Graphene Quantum Dots. *J. Am. Chem. Soc.* **2014**, *136*, 3760-3763.
32. Wang, J. T.-W.; Ball, J. M.; Barea, E. M.; Abate, A.; Alexander-Webber, J. A.; Huang, J.; Saliba, M.; Mora-Sero, I.; Bisquert, J.; Snaith, H. J.; Nicholas, R. J. Low-Temperature Processed Electron Collection Layers of Graphene/TiO_2 Nanocomposites in Thin Film Perovskite Solar Cells. *Nano Lett.* **2013**, *14*, 724-730.
33. Yan, X.; Li, Q.; Li, L.-s. Formation and Stabilization of Palladium Nanoparticles on Colloidal Graphene Quantum Dots. *J. Am. Chem. Soc.* **2012**, *134*, 16095-16098.
34. Scheele, M.; Oeschler, N.; Meier, K.; Kornowski, A.; Klinke, C.; Weller, H. Synthesis and Thermoelectric Characterization of Bi_2Te_3 Nanoparticles. *Adv. Funct. Mater.* **2009**, *19*, 3476-3483.
35. Dresselhaus, M. S.; Chen, G.; Tang, M. Y.; Yang, R. G.; Lee, H.; Wang, D. Z.; Ren, Z. F.; Fleurial, J. P.; Gogna, P. New Directions for Low-Dimensional Thermoelectric Materials. *Adv. Mater.* **2007**, *19*, 1043-1053.
36. Urban, J. J.; Talapin, D. V.; Shevchenko, E. V.; Murray, C. B. Self-Assembly of PbTe Quantum Dots into Nanocrystal Superlattices and Glassy Films. *J. Am. Chem. Soc.* **2006**, *128*, 3248-3255.
37. Cho, K.-S.; Talapin, D. V.; Gaschler, W.; Murray, C. B. Designing PbSe Nanowires and Nanorings through Oriented Attachment of Nanoparticles. *J. Am. Chem. Soc.* **2005**, *127*, 7140-7147.
38. Hines, M. A.; Scholes, G. D. Colloidal PbS Nanocrystals with Size-Tunable Near-Infrared Emission: Observation of Post-Synthesis Self-Narrowing of the Particle Size Distribution. *Adv. Mater.* **2003**, *15*, 1844-1849.
39. Peng, Z. A.; Peng, X. Formation of High-Quality CdTe, CdSe, and CdS Nanocrystals Using CdO as Precursor. *J. Am. Chem. Soc.* **2000**, *123*, 183-184.
40. Xu, Y.; Bai, H.; Lu, G.; Li, C.; Shi, G. Flexible Graphene Films via the Filtration of Water-Soluble Noncovalent Functionalized Graphene Sheets. *J. Am. Chem. Soc.* **2008**, *130*, 5856-5857.
41. Liu, Q.; Guo, B.; Rao, Z.; Zhang, B.; Gong, J. R. Strong Two-Photon-Induced Fluorescence from Photostable, Biocompatible Nitrogen-Doped Graphene Quantum Dots for Cellular and Deep-Tissue Imaging. *Nano Lett.* **2013**, *13*, 2436-2441.
42. Pan, D.; Zhang, J.; Li, Z.; Wu, M. Hydrothermal Route for Cutting Graphene Sheets into Blue-Luminescent Graphene Quantum Dots. *Adv. Mater.* **2010**, *22*, 734-738.
43. El-Ballouli, A. a. O.; Alarousu, E.; Bernardi, M.; Aly, S. M.; Lagrow, A. P.; Bakr, O. M.; Mohammed, O. F. Quantum Confinement-Tunable Ultrafast Charge Transfer at the PbS Quantum Dot and Phenyl-C_{61}-butyric Acid Methyl Ester Interface. *J. Am. Chem. Soc.* **2014**, *136*, 6952-6959.
44. Williams, K. J.; Nelson, C. A.; Yan, X.; Li, L. S.; Zhu, X. Y. Hot Electron Injection from Graphene Quantum Dots to TiO_2. *Acs Nano* **2013**, *7*, 1388-1394.
45. Finefrock, S. W.; Zhang, G. Q.; Bahk, J. H.; Fang, H. Y.; Yang, H. R.; Shakouri, A.; Wu, Y. Structure and Thermoelectric Properties of Spark Plasma Sintered Ultrathin PbTe Nanowires. *Nano Lett.* **2014**, *14*, 3466-3473.
46. Scheele, M.; Oeschler, N.; Veremchuk, I.; Peters, S. O.; Littig, A.; Kornowski, A.; Klinke, C.; Weller, H. Thermoelectric Properties of Lead Chalcogenide Core-Shell Nanostructures. *Acs Nano* **2011**, *5*, 8541-8551.
47. Saraidarov, T.; Reisfeld, R.; Sashchiuk, A.; Lifshitz, E. Synthesis and characterization of PbS nanocrystallites organized into different morphological assemblies. *J. Non-Cryst. Solids* **2004**, *345*, 698-702.
48. Dong, J.; Liu, W.; Li, H.; Su, X.; Tang, X.; Uher, C. In situ synthesis and thermoelectric properties of PbTe-graphene nanocomposites by utilizing a facile and novel wet chemical method. *J. Mater. Chem. A* **2013**, *1*, 12503-12511.
49. Ibanez, M.; Zamani, R.; Gorsse, S.; Fan, J. D.; Ortega, S.; Cadavid, D.; Morante, J. R.; Arbiol, J.; Cabot, A. Core-Shell Nanoparticles As Building Blocks for the Bottom-Up Production of Functional Nanocomposites: PbTe-PbS Thermoelectric Properties. *Acs Nano* **2013**, *7*, 2573-2586.
50. Kovalenko, M. V.; Spokoyny, B.; Lee, J. S.; Scheele, M.; Weber, A.; Perera, S.; Landry, D.; Talapin, D. V. Semiconductor Nanocrystals Functionalized with Antimony Telluride Zintl Ions for Nanostructured Thermoelectrics. *J. Am. Chem. Soc.* **2010**, *132*, 6686-6695.
51. Scheele, M.; Oeschler, N.; Veremchuk, I.; Reinsberg, K.-G.; Kreuziger, A.-M.; Kornowski, A.; Broekaert, J.; Klinke, C.; Weller, H. ZT Enhancement in Solution-Grown $Sb_{(2-x)}Bi_xTe_3$ Nanoplatelets. *Acs Nano* **2010**, *4*, 4283-4291.
52. Zhuo, S.; Shao, M.; Lee, S.-T. Upconversion and Downconversion Fluorescent Graphene Quantum Dots:

Ultrasonic Preparation and Photocatalysis. *ACS Nano* **2012**, *6*, 1059-1064.
53. Dutta, M.; Sarkar, S.; Ghosh, T.; Basak, D. ZnO/Graphene Quantum Dot Solid-State Solar Cell. *J. Phys. Chem. C* **2012**, *116*, 20127-20131.
54. Ye, R.; Xiang, C.; Lin, J.; Peng, Z.; Huang, K.; Yan, Z.; Cook, N. P.; Samuel, E. L. G.; Hwang, C.-C.; Ruan, G.; Ceriotti, G.; Raji, A.-R. O.; Martí, A. A.; Tour, J. M. Coal As an Abundant Source of Graphene Quantum Dots. *Nat. Commun.* **2013**, *4*.
55. Wang, L.; Wang, Y.; Xu, T.; Liao, H.; Yao, C.; Liu, Y.; Li, Z.; Chen, Z.; Pan, D.; Sun, L.; Wu, M. Gram-scale synthesis of single-crystalline graphene quantum dots with superior optical properties. *Nat. Commun.* **2014**, *5*.